









**Multiband superconductivity in V<sub>3</sub>Si determined from studying the response to controlled disorder**Kyuil Cho <sup>1,2</sup>, M. Kończykowski <sup>3</sup>, S. Ghimire <sup>1,2</sup>, M. A. Tanatar <sup>1,2</sup>, Lin-Lin Wang <sup>1</sup>,  
V. G. Kogan <sup>1</sup> and R. Prozorov <sup>1,2,\*</sup><sup>1</sup>Ames Laboratory, Ames, Iowa 50011, USA<sup>2</sup>Department of Physics and Astronomy, Iowa State University, Ames, Iowa 50011, USA<sup>3</sup>Laboratoire des Solides Irradiés, CEA/DRF/IRAMIS, École Polytechnique, CNRS, Institut Polytechnique de Paris, F-91128 Palaiseau, France (Received 25 September 2021; revised 6 December 2021; accepted 14 December 2021; published 7 January 2022)

The London penetration depth  $\lambda(T)$  was measured in a single crystal of V<sub>3</sub>Si. The superfluid density obtained from this measurement shows a distinct signature of two almost decoupled superconducting gaps. This alone is insufficient to distinguish between  $s_{\pm}$  and  $s_{++}$  pairing states, but it can be achieved by studying the effect of controlled nonmagnetic disorder on the superconducting transition temperature  $T_c$ . For this purpose, the same V<sub>3</sub>Si crystal was sequentially irradiated by 2.5-MeV electrons three times, repeating the measurement between the irradiation runs. A total dose of 10 C/cm<sup>2</sup> ( $6.24 \times 10^{19}$  electrons/cm<sup>2</sup>) was accumulated, for which  $T_c$  changed from 16.4 K in a pristine state to 14.7 K (9.3%). Not only is this substantial suppression impossible for a single isotropic gap, but also it is not large enough for a sign-changing  $s_{\pm}$  pairing state. Our electronic band structure calculations show how five bands crossing the Fermi energy can be naturally grouped to support two effective gaps, not dissimilar from the physics of iron pnictides. We analyze the results using two-gap models for both  $\lambda(T)$  and  $T_c$  which describe the data very well. Thus the experimental results and theoretical analysis provide strong support for an  $s_{++}$  superconductivity with two unequal gaps,  $\Delta_1(0) \approx 2.53$  meV and  $\Delta_2(0) \approx 1.42$  meV, and a very weak interband coupling in the V<sub>3</sub>Si superconductor.

DOI: [10.1103/PhysRevB.105.024506](https://doi.org/10.1103/PhysRevB.105.024506)**I. INTRODUCTION**

At the time of its discovery in 1953 [1], a cubic (A15 structure) V<sub>3</sub>Si compound had the highest superconducting transition temperature, around 17 K. Despite showing a clear exponential attenuation of all thermodynamic quantities upon cooling towards  $T = 0$ , which signaled a fully gapped Fermi surface, most spectroscopic [2,3], transport [4,5], and thermodynamic measurements [3,6–8] showed unconventional behavior or at least some unusual features. Such behavior can be associated with a peculiar electronic band structure showing Van Hove singularities in the density of states (DOS) close to the Fermi level [3,9–11]. While this certainly plays an important role, now we know that a multigap superconductivity is needed as well to understand the measurements. Here, we focus on a multiband, multigap nature of superconductivity in this fascinating material.

While MgB<sub>2</sub> [12] is commonly accepted as the first confirmed two-gap superconductor [13–15], the multiband superconductivity was studied much earlier, albeit only theoretically. Soon after the development of the microscopic model of superconductivity [16] the possibility of “overlapping bands” was studied [17–19], eventually leading to a general description of multiband superconductivity [20–23], in particular, the effects of disorder [23]. Nevertheless, before MgB<sub>2</sub>, there was no attempt to interpret the unusual properties of V<sub>3</sub>Si through the prism of multiband effects. The observations of the unconventional London penetration depth

[2,3], the anisotropic upper critical field  $H_{c2}$  [6], an unexpectedly large decrease in  $T_c$  with nonmagnetic disorder, either after neutron irradiation [5,24] or naturally present in real material [25], a large  $T_c/T_F \sim 0.01$  ratio ( $T_F$  is Fermi temperature) [3], and a variety of vortex lattice configurations [26] all pointed to an unconventional behavior of a confirmed  $s$ -wave superconductor. Surely, modern reinterpretation of many of these results is consistent, if not fully explained with multigap superconductivity. Therefore, retrospectively, V<sub>3</sub>Si is “the first” two-band superconductor, much older than MgB<sub>2</sub>.

Experimental observation of a two-gap superconducting state relies on a substantial decoupling between the two bands and a substantial difference between them in terms of dimensionality, electronic properties, pairing mechanism, and/or scattering rates [7,27–29]. In terms of more recent measurements, when multiband superconductivity became widely accepted and discussed, circa 2001, while some reports support single-gap conventional  $s$ -wave Bardeen-Cooper-Schrieffer (BCS) superconductivity in V<sub>3</sub>Si [28], many more experimental and theoretical studies point to two distinct energy gaps in this material [7,30–32]. There is a complication, though. Perhaps due to a variation of stoichiometry, atomic disorder, or the extremely strain-sensitive structure of Van Hove singularities in the vicinity of the Fermi level, V<sub>3</sub>Si samples show a spread of behaviors, especially in the properties related to a two-gap superconductivity [4,8,10,11,24,30,33]. Furthermore, establishing a multiband nature from thermodynamic measurements is necessary but insufficient for the microscopic understanding of superconductivity, because the order parameter enters thermodynamic quantities in the even powers and therefore

\*prozorov@ameslab.gov

the gaps of the same or opposite signs on different bands contribute similarly [7,27,34,35]. In this situation, phase-sensitive experiments are needed, but such experiments are often difficult or impossible to devise depending on a superconductor [22,36,37]. While in high- $T_c$  cuprates direct measurements that depend on the phase variation along the Fermi surface have provided a definitive proof of a sign-changing  $d$ -wave order parameter [36], in multiband iron-based superconductors, a similar simple arrangement in real space is not possible, and more complicated approaches are needed [37]. The interpretations of more complex phase-sensitive experiments, such as quasiparticles interference, are not straightforward either [38,39].

Scattering off nonmagnetic impurities is a phase-sensitive method, albeit indirect, that was successfully used in iron-based superconductors to probe the sign-changing multiband  $s_{\pm}$  order parameter [40–42]. As we discuss in Sec. III E, the suppression of  $T_c$  formally depends on the Fermi surface averaging of the order parameter in the first power,  $\langle \Delta(\mathbf{k}) \rangle_{\text{FS}}$ , which is sign sensitive. For example, the isotropic  $s$ -wave angular part averages to 1, but the  $d$  wave averages to 0. Of course, more than one measurement is needed for different levels of scattering in the system. In our approach, simultaneous measurements of normal-state resistivity (to characterize the amount of introduced disorder), superconducting transition temperature  $T_c$  (phase-sensitive measurement), and low-temperature variation of the London penetration depth  $\lambda(T)$  (to estimate the anisotropy of the order parameter amplitude) provide enough information to make that conclusion. Here, we show that this scheme can be applied to prove the existence of two distinct gaps of the same sign, or  $s_{++}$  order parameter, in the title material,  $\text{V}_3\text{Si}$ . The utility of such an approach was extended significantly by recent theoretical analysis of the impurity scattering in superconductors with nontrivial multiband structure [43,44]. For example, it is possible to have a singlet unconventional pairing with a sign-changing superconducting order parameter, yet fully gapped Fermi surface, similar to what we uncover here. However, the electronic band structure should support such an unconventional scenario in the first place. We note that nodeless unconventional superconductivity has been studied in the context of triplet pairing, such as the  $p$  wave, which shows a variety of nodal and nodeless behaviors depending on the material and experimental conditions, for example, in some heavy-fermion superconductors [45,46]. However, most superconductors have singlet pairing states, and studies of the effects of controlled disorder are a powerful tool to study unconventional and exotic states, including multigap superconductivity [42]. For example, a similar combination of London penetration depth measurements of electron-irradiated samples was used to study disorder-driven transitions of the superconducting gap [47], to study the interplay of ferromagnetism and superconductivity [48], to prove fully gapped superconductivity in a heavy-fermion superconductor [49], and to follow the doping evolution of the order parameter [50]. If we include other types of irradiation, many studies employed neutrons and protons to induce nonmagnetic disorder. Such disorder was used to induce a two-gap-to-single-gap crossover in  $\text{MgB}_2$  [51], to trace the evolution of  $s_{\pm}$  symmetry in iron pnictides

[52] and study its crossover to the  $s_{++}$  state [41], and to significantly suppress the superfluid density [53]. Evidently, controlled disorder in conjunction with thermodynamic measurements is a well-established approach to tune and probe the superconducting state.

## II. EXPERIMENT

Our  $\text{V}_3\text{Si}$  crystals with  $T_c \approx 16.4$  K were cut out of a “master boule” single crystal studied previously, for example, in Refs. [54,55] and references therein. The resistivity above  $T_c$  of pristine samples was in the range of 5–10  $\mu\Omega$  cm, consistent with previous reports [25,54,55]. The samples were of submillimeter size. In particular, the crystal used in the electron irradiation study was  $0.73 \times 0.62 \times 0.20$  mm<sup>3</sup>.

The variation of the in-plane London penetration depth  $\Delta\lambda(T)$  was measured using a self-oscillating tunnel-diode resonator (TDR) technique [27,34,56]. The TDR circuit resonates approximately at 14 MHz, and the frequency shift is measured with a precision better than one part per 10<sup>9</sup> (1 ppb). Its inductor coil generates an ac magnetic field,  $H_{\text{ac}} < 20$  mOe, so that the sample is always in the Meissner state at the temperatures of interest. Details of the technique and its principles are given in Refs. [57–59], and the detailed calibration procedure is described in Refs. [58,60]. The sample was mounted on a 1-mm-diameter sapphire rod and inserted into a 2-mm-diameter inductor coil. The coil and the sample were mounted in vacuum inside a <sup>3</sup>He cryostat. The TDR circuit was actively stabilized at 5 K, and the sample was controlled from 0.4 K and up by independent LakeShore controllers. It is straightforward to show that the change in the resonant frequency when a sample is inserted into the coil is proportional to the sample magnetic susceptibility as long as the change in the total inductance is small and one can expand,  $\Delta f/f_0 \approx \Delta L/2L_0$ , where  $2\pi f_0 = 1/\sqrt{CL_0}$  with subindex “0” referring to an empty resonator. The coefficient of proportionality that includes the demagnetization correction is measured directly by pulling the sample out of the resonator at the base temperature [60].

The low-temperature 2.5-MeV electron irradiation was performed at the SIRIUS Pelletron facility of the Laboratoire des Solides Irradiés (LSI) at the École Polytechnique in Palaiseau, France. The acquired irradiation dose is conveniently expressed in C/cm<sup>2</sup> and measured directly as a total charge accumulated behind the sample by a Faraday cage. Therefore 1 C/cm<sup>2</sup>  $\approx$  6.24  $\times$  10<sup>18</sup> electrons/cm<sup>2</sup>. In the experiment, the London penetration depth was measured, then the sample was irradiated, and the cycle repeated. The irradiation was carried out with the sample immersed in liquid hydrogen at about 20 K. Low-temperature irradiation is needed to slow down recombination and migration of defects. Upon warming up to room temperature, a quasiequilibrium population of atomic vacancies remains due to a substantial difference in the migration barriers between vacancies and interstitials. An example of such an incremental irradiation and measurement sequence showing the resistivity change measured *in situ*, as well as the annealing after warming up, is given elsewhere [61]. In the present case, the sample was dispatched between the laboratory and the irradiation facility for the measurements and irradiation, and then the sequence

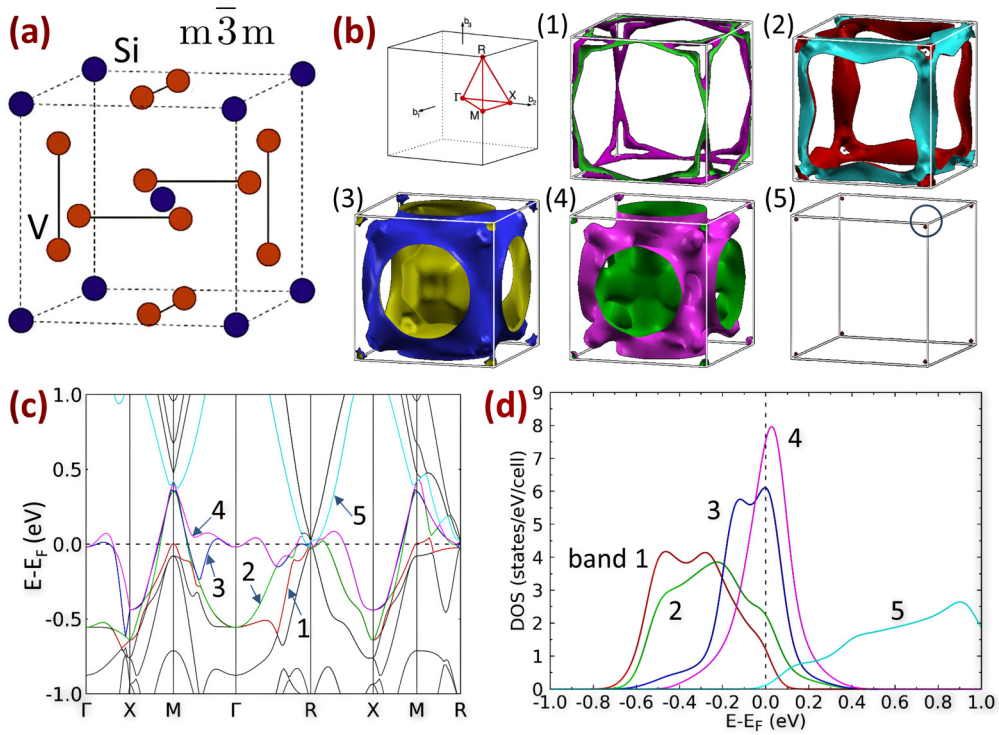


FIG. 1. (a)  $V_3Si$  unit cell with two formula units,  $Z = 2$ . (b) Brillouin zone (BZ) and Fermi surfaces (FS) of the five different bands crossing the Fermi level ( $E_F$ ) for  $V_3Si$ . The band numbers (bands 1–5) correspond to the numbers in the text. (The small FS of band 5 is circled for clarity.) (c) Energy band dispersion along the high-symmetry directions of the BZ. (d) Partial density of states as a function of energy for the five bands crossing  $E_F$ .

was repeated until the sample had accumulated a substantial dose of  $10 \text{ C/cm}^2 \approx 6.24 \times 10^{19} \text{ electrons/cm}^2$ . Further information on the physics of electron irradiation can be found elsewhere [62,63].

Density functional theory (DFT) with Perdew-Burke-Ernzerhof (PBE) exchange-correlation functional [64] has been used to calculate the band structure of  $V_3Si$  at the experimental lattice constant of  $a = 4.741 \text{ \AA}$  [65]. The DFT calculations have been done using the Vienna *ab initio* simulation package (VASP) [66] in the projected augmented wave method and a plane-wave basis set with a kinetic energy cutoff of 246 eV. The charge density is converged on a  $(8 \times 8 \times 8)$  Monkhorst-Pack  $k$ -point mesh, including the  $\Gamma$  point. For the Fermi surface (FS) calculations, a much denser  $(30 \times 30 \times 30)$   $k$ -point mesh is used. The Fermi velocity for each band has been calculated by the derivative of the DFT band dispersion, i.e., group velocity, and then averaged over the Fermi surface of each band in the Brillouin zone (BZ), the same method as employed previously [67,68].

### III. RESULTS AND DISCUSSION

#### A. Electronic band structure

$V_3Si$  has a primitive cubic crystal structure in space group 223 ( $Pm\bar{3}n$ ) with V sitting at the 6c positions and Si at the 2a positions as shown in Fig. 1(a). The band structure of  $V_3Si$  [Fig. 1(c)] has flat pieces along the  $\Gamma$ -X,  $\Gamma$ -M, and  $\Gamma$ -R directions, which is similar to  $Nb_3Sn$ , another A15 superconductor with the same, group V, transition metal. There are five

bands crossing the  $E_F$  as highlighted in different colors in Fig. 1(c). The corresponding partial densities of states (DOS) of these bands are plotted in Fig. 1(d) and summarized in Table I. Among them, bands 1 and 2 are hole bands with states gathering along the  $M$ -R direction, the edges of the cubic BZ [see Fig. 1(b), bands 1 and 2]. On the other hand, band 5 has a very small electron pocket around the R point, and the contribution to the DOS is negligibly small. In contrast, bands 3 and 4 are dominant in the DOS at  $E_F$ , which corresponds to most of the flat-band contributions around the  $\Gamma$  point as seen in Fig. 1(c). The three-dimensional (3D) FSs in Fig. 1(b) show complex FSs for both bands 3 and 4, which have multiple sheets at  $E_F$ . Analysis of Fig. 1(b) suggests that the five bands can be naturally grouped into two effective ones. Specifically, bands 1 and 2 are well separated in energy from bands 3 and 4 at intermediate  $k$  values inside the BZ, making the interband transitions improbable. Furthermore, bands 1 and 2 are much closer in energy, and this is also true for bands 3 and 4, but at different  $k$ . This suggests grouping bands 1 and 2 into an effective, band I; grouping bands 3 and 4 into another effective, band II; and discarding negligible-DOS band 5. Electronic parameters of all five bands are reported in Table I. The “effective” parameters of the two effective bands, bands I and II, are given in the last two columns. The multiband average for band I is  $v_{F,I}^2 = (n_1 v_{F,1}^2 + n_2 v_{F,2}^2)/(n_1 + n_2)$ , and similar for effective band II. As we explain in the two-band  $\gamma$ -model section, Sec. III C, the relative contribution of each band to the superfluid density,  $\rho_s = \gamma \rho_I + (1 - \gamma) \rho_{II}$ , is given by the parameter  $\gamma = n_1 v_I^2 / (n_1 v_I^2 + n_{II} v_{II}^2)$  (hence the  $\gamma$  model). As

TABLE I. Electronic band structure parameters relevant to the  $\gamma$ -model fitting. The bands are naturally grouped into two effective bands, bands I and II. The calculated parameter  $\gamma = (n_1 v_1^2 + n_2 v_2^2) / \sum_{i=1}^5 n_i v_i^2 = n_1 v_1^2 / (n_1 v_1^2 + n_{II} v_{II}^2) = 0.109$ , to be compared with the experimental best fit,  $\gamma = 0.175$ . The effective quantities remapped on the two effective bands are shown in the last two columns.

Band	$10^{15} v_F^2$ (cm/s) <sup>2</sup>	DOS (states eV <sup>-1</sup> cell <sup>-1</sup> )	Two bands	$10^{15} v_F^2$ (cm/s) <sup>2</sup>	DOS (states eV <sup>-1</sup> cell <sup>-1</sup> )
1	2.22	1.22	I	3.69	1.74
2	4.48	2.26			
3	7.11	6.11	II	7.70	6.80
4	8.18	7.48			
5	0.00315	0.11			

shown in Table I, we estimate  $\gamma = 0.109$ , which is quite close to the experimental  $\gamma = 0.175$ , as discussed in Sec. III C.

The high DOS at  $E_F$  in  $V_3Si$  indicates electronic instability, consistent with literature reports [3,10,11]. Although one way to reduce such instability is to promote an exchange splitting, giving a magnetic solution at the DFT level, experimentally  $V_3Si$  is not magnetic. Another way to lift the electronic instability is through the electron-phonon coupling. A similar band structure with flat bands in  $Nb_3Sn$  is susceptible to lattice distortion by a phonon mode [69], indicating a strong electron-phonon coupling in such compounds and hence an obvious connection to superconductivity. Thus the nonmagnetic electronic band structure of  $V_3Si$  provides important microscopic details for superconductivity models, such as DOS at  $E_F$  and Fermi velocity, which have been used successfully for  $MgB_2$ , the first proven two-band superconductor. In fact, we calculated the electronic band structure of  $MgB_2$  as a benchmark to compare with the original  $\gamma$  model [7,29] and one of the first DFT calculations of a two-gap system [67], and obtained similar results.

### B. London penetration depth and superfluid density

We begin by examining the superfluid density obtained from the measured London penetration depth. Figure 2 shows the temperature-dependent variation of London penetration depth,  $\Delta\lambda \equiv \lambda(T) - \lambda(T_{\min})$ , with the increasing dose of electron irradiation. Considering the exponential low-temperature behavior, we can safely assume that  $\lambda(T_{\min} = 0.4 \text{ K}) \approx \lambda(0)$ , and then the normalized superfluid density is calculated as  $\rho_s = (\Delta\lambda(0)/\Delta\lambda(T))^2 = (1 + \Delta\lambda/\lambda(0))^{-2}$ . The inset in Fig. 2 zooms in on the low-temperature region. There is a clear, almost kneelike feature in  $\Delta\lambda(T)$  around 10 K, which we now know is expected for a two-gap superconductor with different and weakly coupled gaps [27]. Similar features were reported in high-quality  $V_3Si$  crystals before and not surprisingly were interpreted as definitive evidence of a two-gap superconductivity [7,30]. The temperature of this kinklike feature is suppressed upon irradiation approximately at the same rate as  $T_c$ , signaling that both gaps change at a similar rate. Furthermore, in Fig. 2, normal-state values above  $T_c$  are determined by the skin depth. They increase upon irradiation due to the increase in residual resistivity following the Matthiessen's rule [70]. Importantly, the superconducting transition temperature  $T_c$  is monotonically and noticeably suppressed from 16.4 to 14.7 K (9.3%). The upper cutoff

at  $T_c$  is determined by the normal-metal skin depth, which allows us to estimate the resistivity in a contactless way using  $\rho = \mu_0 \pi f \delta^2$  where  $\delta(T_c \leftarrow T) \approx 2\lambda(T \rightarrow T_c)$  and  $\lambda(T) = \Delta\lambda(T) + \lambda(0)$ , where  $\lambda(0) = 130 \text{ nm}$  from Refs. [3,4]. The extracted resistivity values are 8.6, 11, 13.6, and  $15.4 \mu\Omega \text{ cm}$  for 0, 2.1, 5.7, and  $10 \text{ C/cm}^2$  electron irradiation doses, respectively. These values appear to be quite comparable to those of the literature [4,5,25]. We note that in a large body of work on  $V_3Si$ , a spread of  $\lambda(0)$  values ranging from 83 to 230 nm can be found. They were obtained using different methods and in samples of different forms (crystal vs polycrystalline) and purity [71–73]. The value we use is within the statistical maximum of the current literature values. Importantly, our results and conclusions are independent of the particular value of  $\lambda(0)$ .

Figure 3(a) shows the normalized superfluid density of a  $V_3Si$  crystal in pristine state. A similar curve for a different crystal, cut from the same master boule, showing the same two-gap structure, was published in our earlier paper, where a self-consistent  $\gamma$  model based on Eilenberger formalism was introduced [7]. In the original  $\gamma$  model, two isotropic  $s$ -wave gaps are obtained from the solution of the self-consistency equation, and then all thermodynamic quantities, including the superfluid density, can be calculated. The model was

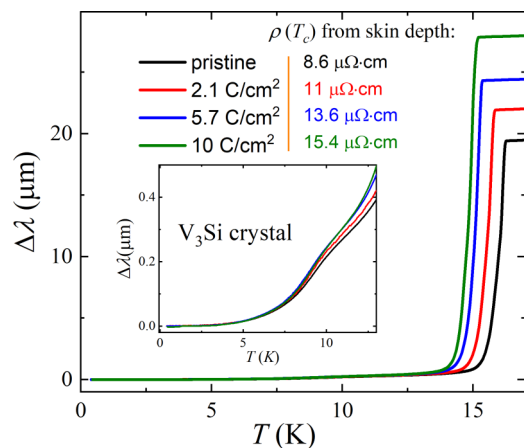


FIG. 2. Temperature-dependent London penetration depth measured in a  $V_3Si$  single crystal in pristine state and after three doses of electron irradiation. The inset zooms in on the low-temperature region showing a clear signature of a second gap developing at around 10 K.



further generalized to include anisotropic or even nodal gaps [74]. Here, it is sufficient to consider the original isotropic approach.

### C. The isotropic $\gamma$ model

The  $\gamma$  model considers two bands with Fermi velocities  $v_i$  and partial densities of states  $n_i = N_i(0)/N(0)$ , where  $N(0)$  is the total density of states at the Fermi level, so that  $n_1 + n_2 = 1$ . The dimensionless effective interaction constants are defined as  $v_{ik} = N(0)V_{ik}$ , where  $V_{ik}$  is the electron-electron interaction matrix. Note that in Ref. [7] we used  $\lambda$  for the interaction matrix. To avoid confusion with the London penetration depth, here we use  $v_{ik}$ . Also note that this definition differs from that used in the literature,  $g_{ik} = n_k v_{ik}$ . Our notation has the advantage of being symmetric,  $v_{ik} = v_{ki}$ . Therefore, for two bands, we have three coefficients of the interaction matrix, two in-band coefficients,  $v_{11}$  and  $v_{22}$ , and an inter-band coupling coefficient,  $v_{12}$ . In the analysis, we perform a least-squares fit of the experimental superfluid density shown in Fig. 3(a) in MATLAB. If all normal-state parameters of a material are known, the coupling constants  $v_{ik}$  are the three fitting parameters. They are reduced to two free parameters by the equation for  $T_c(v_{ik})$ ,

$$1.7638k_B T_c = 2\hbar\omega_D \exp(-1/\tilde{v}), \quad (1)$$

where we assume the conventional electron-phonon mechanism of superconductivity with  $\omega_D$  being the Debye frequency. In general, if the energy of the bosonic pairing ‘‘glue’’ is known, it should be substituted instead of  $\hbar\omega_D$  in Eq. (1). The prefactor comes from the weak-coupling approximation used in the  $\gamma$  model. The effective interaction constant  $\tilde{v}(v_{ik})$  is obtained from the solution of algebraic equations containing all coefficients,  $v_{ik}$ ; see Sec. II A of Ref. [7]. To fit the superfluid density, first the self-consistent gap equation is solved at each temperature. Introducing dimensionless quantities,  $\delta_i = (\Delta_i/T)/(2\pi t)$ , where  $t = T/T_c$ , the gap equations are given by

$$\delta_i = \sum_{k=1,2} n_k v_{ik} \delta_k (\tilde{v}^{-1} - \ln t - A_k),$$

$$A_k = \sum_{n=0}^{\infty} [(n+1/2)^{-1} - (\delta_k^2 + (n+1/2)^2)^{-1/2}]. \quad (2)$$

Note that we often set the Boltzmann constant  $k_B = 1$  where it is obvious and use it explicitly to emphasize the numerical values or proper dimensions, e.g., Eq. (1). For a given set of the coupling constants  $v_{ik}$  and partial densities of states  $n_i$ , this system can be solved numerically for  $\delta_i(t)$  and therefore provide the energy gaps  $\Delta_i(t) = 2\pi T \delta_i(t)$ . This is a crucial step missing in the so-called  $\alpha$ -model description of two-band superconductivity [13]. While it was useful early on to explain experimental signatures of two-gap superconductivity in MgB<sub>2</sub>, the fitting parameters of the  $\alpha$  model have little physical meaning. A follow-up study used two-gap functions precalculated from the microscopic theory and showed an excellent agreement between experimental and theoretical superfluid density  $\rho_s(t)$  [75]. Indeed, the  $s$ -wave MgB<sub>2</sub>, for which all normal-state parameters are known, is a perfect

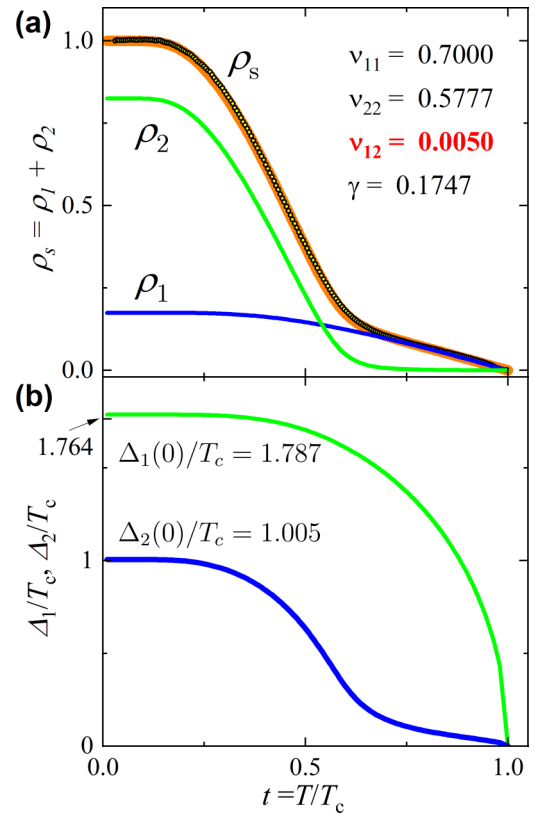


FIG. 3. (a) Symbols show the superfluid density in pristine sample calculated from the data shown in Fig. 2. Blue and green solid curves show labeled partial superfluid densities,  $\rho_1$  and  $\rho_2$ , obtained in the least-squares fitting. The thick orange curve behind the data shows an excellent agreement of the data with the fitted total superfluid density,  $\rho_s = \gamma\rho_1 + (1-\gamma)\rho_2$ . Best-fit parameters are  $v_{11} = 0.700$ ,  $v_{22} = 0.578$ ,  $v_{12} = 0.005$ , and  $\gamma = 0.175$ . (b) Best-fit solutions of the self-consistency gap equations, Eq. (2). The  $T = 0$  gap ratios are  $\Delta_1/T_c = 1.787$  and  $\Delta_2/T_c = 1.005$ .

demonstration of the  $\gamma$  model, where different quantities are calculated from  $v_{ik}$  obtained from the fit of  $\rho_s(t)$  [7,29].

Figure 3(b) shows two gaps calculated self-consistently from Eq. (2). The individual gap ratios are  $\Delta_1/T_c = 1.787$  and  $\Delta_2/T_c = 1.005$ . This should be compared with the results of microwave surface impedance measurements, where similar apparent two-gap behavior was observed in the superfluid density and values of  $\Delta_1/T_c = 1.8$  and  $\Delta_2/T_c = 0.95$ , quite close to ours, were derived [30]. In absolute units we obtain  $\Delta_1(0) \approx 2.53$  meV and  $\Delta_2(0) \approx 1.42$  meV. After the gaps are calculated, the total superfluid density,  $\rho_s = \gamma\rho_1 + (1-\gamma)\rho_2$ , can be evaluated and fitted to the experimental data. The partial contributions to the superfluid density are given by [7]

$$\rho_i = \delta_i^2 \sum_{n=0}^{\infty} [\delta_i^2 + (n+1/2)^2]^{-3/2},$$

$$\gamma = \frac{n_1 v_1^2}{n_1 v_1^2 + n_2 v_2^2}, \quad (3)$$

where  $v_i$  are the Fermi velocities (not to be confused with Greek  $v_i$  of the interaction matrix). Analyzing Fig. 1, we group bands 1 and 2 into one effective band I and bands 3

and 4 into another band, band II, and we can safely neglect band 5. (Here, we use Roman numerals I and II to index these “effective” bands.) For the first effective band, we find  $\gamma = (n_1 v_1^2 + n_2 v_2^2) / \sum_{i=1}^5 n_i v_i^2 = 0.109$ . If we included band 5, it would make a difference only in the sixth decimal digit. Using  $\gamma$  as another fitting parameter, the best fit of this model to the data gave  $v_{11} = 0.700$  [fixed by  $T_c$ , Eq. (1)],  $v_{22} = 0.578$ ,  $v_{12} = 0.005$ , and  $\gamma = 0.175$ , with the effective  $\tilde{v} = 0.350$  [see Eq. (1)]. Remarkably, the best-fit value of  $\gamma$  is quite close to the estimate from the electronic band structure calculations; see Table I, where we find  $\gamma = 0.109$ . This gives confidence in the model and shows its applicability to describe the superconductivity in  $V_3Si$ . Naturally, overall, a smaller partial density of states on band I, somewhat counterintuitively, leads to a larger gap, which is the property of the self-consistent two-band model [7,35]. We note that the possible uncertainty in the experimental value of  $\lambda(0)$  leads to some uncertainty in the fitting parameters, but not large enough to alter the general conclusion of the relative amplitudes of the obtained interaction matrix.

#### D. Effect of electron irradiation

In the last three decades, many studies involving particle irradiation were performed on various conventional and unconventional superconductors, and there is a vast literature on this topic [42,76–78]. Due to the differences in the rest mass and irradiation temperature, the number and the morphology of the created defects vary significantly between different projectile particles. It appears that MeV electrons, thanks to a small rest mass, transfer just enough energy upon collision with ions, of the order of tens of eV, to produce well-defined pointlike scattering centers [48]. Much larger energy transfer, for example, from protons, produces many secondary collisions and less localized damage. A more detailed discussion of electron irradiation and created defects in solids can be found elsewhere [62,63].

Figure 4 shows the ion-type-resolved cross sections of the defect creation calculated using Sections Efficaces Calcul Transport d’Électrons (SECTE) software, developed at École Polytechnique (Palaiseau, France) by members of the Laboratoire des Solides Irradiés, specifically for the interpretation of MeV-range electron irradiation using their Pelletron-type accelerator, SIRIUS [79]. Basically, this is a computer-assisted atomic-weight-averaged interpolation of the ion knockout cross sections tabulated by Oen [80]. In the absence of microscopic calculations, we used the commonly assumed value of the ion displacement energy upon a head-on collision,  $E_d = 25$  eV. The partial cross sections are very similar, and we expect a roughly equal number of defects on vanadium and silicon sites. At the operational energy of 2.5 MeV, the total cross section is estimated as  $\sigma_{\text{tot}} = 72$  barns, which means that a dose of  $1 \text{ C/cm}^2$  produces roughly 1.8 defects per 1000 formula units (f.u.). This is a small number of defects that cannot change the electronic structure in any appreciable way, and the significant reduction in  $T_c$  observed in our experiments must have a different explanation, such as its pair-breaking nature.

First, let us examine the effect of electron irradiation on superfluid density. While we do not know how much  $\lambda(0)$

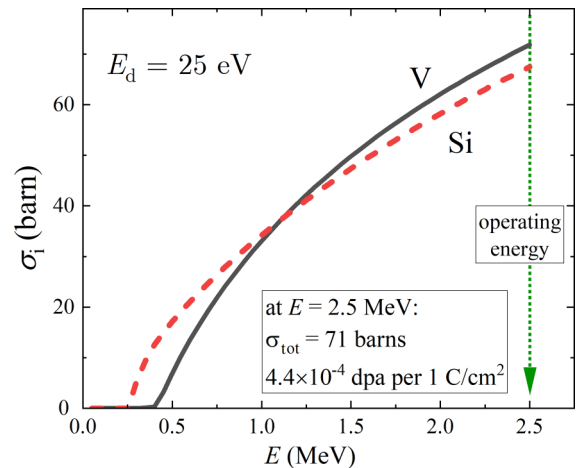


FIG. 4. Knockout defect creation cross sections for vanadium and silicon ions in  $V_3Si$  as a function of electron energy assuming the displacement energy threshold  $E_d = 25$  eV. At the operating energy of 2.5 MeV, the total cross section is  $\sigma_{\text{tot}} = 71$  barns, which leads to an estimate of  $4.4 \times 10^{-4}$  displacements per atom (dpa) per  $1 \text{ C/cm}^2$  of irradiation.

changes, we attempted to adjust its value to scale all curves onto a pristine one. As shown in Fig. 5 this worked rather well with a small increase in  $\lambda(0)$  values shown in the legend. This indicates that scattering does not alter the gap values themselves and, due to very small interband coupling, has practically no effect on the total superfluid density. Each isotropic band follows the Anderson theorem [81], and the change in  $T_c$  comes mostly from the interband scattering between order parameters of different magnitude. We note that the relative change in  $\lambda(0)$  can be estimated from Tinkham’s widely used approach [82], which gives, for moderate scattering,  $\lambda \approx \lambda_{\text{clean}} \sqrt{1 + \xi_0/\ell}$ , where  $\xi_0 \approx 60$  nm is the BCS coherence length and  $\ell \approx 30$  nm is the electronic mean free path in the pristine state. Both numbers are estimated for  $V_3Si$

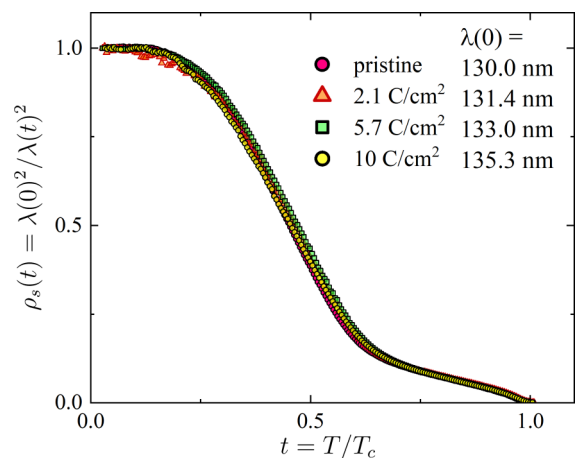


FIG. 5. Evolution of superfluid density  $\rho_s$  upon irradiation. For the pristine case, we used  $\lambda(0) = 130$  nm from Ref. [3]. The curves representing the irradiated state were calculated with the penetration depth  $\lambda(0)$  values shown in the legend. They were chosen to collapse the curves on the pristine one.

from  $T_c$ , Fermi velocity, and resistivity; see Table I and Fig. 2. As shown in Fig. 2, at the maximum irradiation dose, the resistivity doubles. Therefore we expect the increase in  $\lambda(0)$  by a factor of about 1.3, which is not large and does not alter our conclusions, especially considering an apparent scaling shown in Fig. 5.

### E. Suppression of $T_c$ by disorder in a two-band superconductor

While it is clear that the superfluid density shows a convincing two-distinct-gaps feature implying small interband coupling, this still leaves an unanswered important question of the relative sign of the order parameter on each band. This is because superfluid density, as well as any other thermodynamic quantity, includes even powers of the gap function, so that an  $s_{\pm}$  state cannot be distinguished from an  $s_{++}$  state if the gaps are the same; see, for example, Eq. (3). The suppression of  $T_c$ , on the other hand, is very sensitive to the overall anisotropy of the order parameter, including a generalized view when two bands are considered side by side along the common path on the entire Fermi surface [83]. This situation can be analyzed employing a very useful ansatz that temperature and angular parts of the order parameter can be separated,  $\Delta(T, \mathbf{k}_F) = \Psi(T)\Omega(\mathbf{k}_F)$ , where  $\mathbf{k}_F$  is the Fermi wave vector and the angular part obeys the normalization condition for the Fermi surface average,  $\langle \Omega^2 \rangle_{\text{FS}} = 1$  [83,84]. For example, for a single-band  $s$  wave,  $\Omega = 1$ , and for a  $d$  wave,  $\Omega = \sqrt{2} \cos(2\varphi)$ . For a two-gap superconductor, Kogan introduced a simple model in which each band is represented by its own  $\Omega_i$ . We call it the ‘‘Omega approach’’ or ‘‘Omega model’’ [83]. In this case, the normalization reads

$$\langle \Omega^2 \rangle = n_1 \Omega_1^2 + n_2 \Omega_2^2 = 1. \quad (4)$$

In the case of an anisotropic gap, even nonmagnetic (no-spin-flip) scatterers suppress the superconducting transition temperature  $T_c$ . With spin-flip scattering both channels reduce  $T_c$ . Openov gives a generalized expression of Abrikosov-Gor’kov [85] type where gap anisotropy is explicitly taken into account [86,87]. We note that a more general theory of the  $T_c$  suppression by disorder scattering, extended to topologically nontrivial superconductors, is discussed elsewhere [43,44]. Here, it suffices to consider the  $\Omega$  approach, which gives

$$\ln t_c = \psi\left(\frac{g + g_m}{2t_c} + \frac{1}{2}\right) - \psi\left(\frac{1}{2}\right) - \langle \Omega \rangle^2 \left[ \psi\left(\frac{g + g_m}{2t_c} + \frac{1}{2}\right) - \psi\left(\frac{g_m}{t_c} + \frac{1}{2}\right) \right], \quad (5)$$

where  $t_c = T_c/T_{c0}$ , with  $T_{c0}$  being the transition temperature in a pristine state, and  $\psi$  is the digamma function. Dimensionless magnetic and nonmagnetic scattering parameters are given by

$$g_{(m)} = \frac{\hbar}{2\pi k_B T_{c0}} \frac{1}{\tau_{(m)}}, \quad (6)$$

where  $\tau$  and  $\tau_m$  are nonmagnetic and magnetic (spin flip) scattering times, respectively. [Note that the original Abrikosov-Gor’kov theory uses a different definition of the scattering parameter,  $\rho = \hbar/(\pi k_B T_c \tau)$ , with the actual (suppressed)  $T_c$ .] The effect of gap anisotropy can be immediately

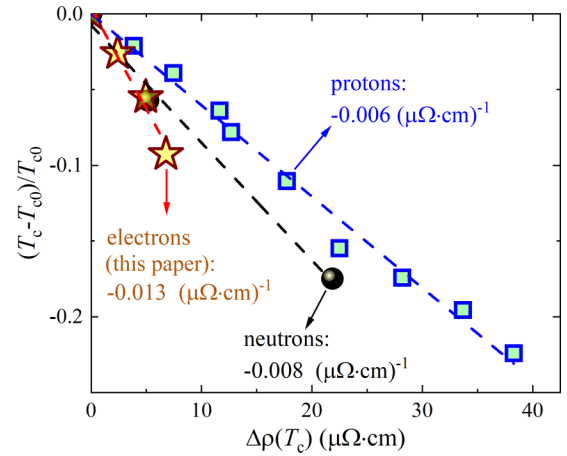


FIG. 6. Suppression of  $T_c$  upon different types of particle irradiation. Normalized  $T_c$  suppression upon electron irradiation (this paper) is compared with two different previous studies using proton [88] and neutron [5] irradiation. It is clearly shown that the electron irradiation is most effective in suppressing  $T_c$ .

seen from Eq. (5): it contains  $\Omega$  in the first power. For a single-band  $s$  wave,  $\langle \Omega \rangle = 1$ , and we obtain  $t_c = 1$ , recovering the Anderson theorem [81]. For a  $d$  wave,  $\langle \Omega \rangle = 0$ , and we obtain an expression where both magnetic and nonmagnetic impurities suppress  $T_c$ . It is instructive to note that the critical value for the complete  $T_c$  suppression of an  $s$ -wave order parameter by magnetic impurities,  $g_m = 0.14$ , is exactly half of the value for a  $d$ -wave order parameter suppression by nonmagnetic impurities,  $g = 0.28$ .

We can now use Eq. (5) with the two-gap  $\Omega$  approach, in which  $\langle \Omega \rangle = n_1 \Omega_1 + n_2 \Omega_2$ . Specifically, we consider two isotropic gaps described by constant values  $\Omega_1$  and  $\Omega_2$ . Introducing the gap ratio  $r = \Omega_2/\Omega_1$  and the ratio of the partial densities of state  $n = n_2/n_1 = N_1/N_2$ , we obtain for the total average in this two-gap model

$$\langle \Omega \rangle^2 = \frac{(nr + 1)^2}{(n + 1)(nr^2 + 1)}. \quad (7)$$

Hence, without magnetic scattering ( $g_m = 0$ ), the transition temperature of a two-band superconductor is given by,

$$\ln t_c = \psi\left(\frac{g}{2t_c} + \frac{1}{2}\right) - \psi\left(\frac{1}{2}\right) - \frac{(nr + 1)^2}{(n + 1)(nr^2 + 1)} \left[ \psi\left(\frac{g}{2t_c} + \frac{1}{2}\right) - \psi\left(\frac{1}{2}\right) \right]. \quad (8)$$

It is important to emphasize that the superfluid density as a function of (reduced) temperature and  $T_c$  are two independent measurements, which makes the analysis better defined and constrained.

To compare the experimentally observed decrease in  $T_c$  with our model, we need a proper parameter characterizing the scattering rate. The problem is that different sources of disorder produce somewhat different effects. Figure 6 compares the relative change in the transition temperature,  $\Delta t_c \equiv (T_c - T_{c0})/T_{c0}$ , in V<sub>3</sub>Si per  $1 \mu\Omega \text{ cm}$  of resistivity increase caused by electron irradiation in this paper with two previous studies where defects were induced by proton [88] and neutron [5]

irradiation. The rates of the relative change are  $d\Delta t_c/d\rho = -0.013(\mu\Omega\text{cm})^{-1}$  (electron irradiation),  $-0.008(\mu\Omega\text{cm})^{-1}$  (neutron irradiation), and  $-0.006(\mu\Omega\text{cm})^{-1}$  (proton irradiation). Due to their small rest mass and matching range of the energy transfer (1–100 eV), electrons produce the most efficient pointlike defects and have the largest suppression rate. A similar trend is observed in other materials, for example, well-studied iron-based superconductors [42,48]. On the other hand, the observed rates are not too different, roughly  $0.01(\mu\Omega\text{cm})^{-1}$ , and we can put it in perspective by comparing with other superconductors. For that, we need to calculate the dimensionless scattering rate, Eq. (6). In our case of measured  $\lambda(T)$  and  $\rho(T)$  the simplest estimate of the scattering time  $\tau$  is via the London and Drude electrodynamics,  $\tau(T_c) = \mu_0\lambda_{\text{clean}}^2(0)/\rho(T_c)$ . Note that the clean-limit value,  $\lambda_{\text{clean}}(0)$ , needed for the density of states in the normal metal, enters this estimate, whereas (normal metal) scattering time comes from resistivity. This approach is well justified in isotropic  $s$ -wave superconductors and  $s_{++}$  compounds assuming that the gap smearing caused by the modest amounts of nonmagnetic disorder is much smaller than the gap amplitudes.

In our case, we can use Tinkham's widely used approach [82],  $\lambda \approx \lambda_{\text{clean}}\sqrt{1 + \xi_0/\ell}$ , which provides a remarkably good agreement with the exact BCS formulas [89,90] in a wide range of the scattering rate from clean to dirty limit. Here,  $\xi_0 \approx 60$  nm is the BCS coherence length and  $\ell \approx 30$  nm is the electronic mean free path in the pristine state. Both numbers are estimated for  $\text{V}_3\text{Si}$  from  $T_c$ , Fermi velocity, and resistivity; see Table I and Fig. 2. As shown in Fig. 2, at the maximum irradiation dose, the resistivity doubles. Therefore we expect an increase in  $\lambda(0)$  by a factor of about 1.3. This is an insignificant change to alter the main features reported here: the exponential attenuation at low temperatures and a higher-temperature kink signaling two barely coupled gaps of different magnitude. This is further confirmed by the apparent scaling of the superfluid density for all doses of electron irradiation (Fig. 5).

The experimental dimensionless scattering rate can be estimated as

$$g \approx \frac{\hbar}{2\pi k_B \mu_0} \frac{\rho(T_c)}{T_{c0} \lambda_{\text{clean}}(0)^2}. \quad (9)$$

Note that we measure resistivity change with respect to the pristine sample to subtract inelastic scattering, but this also removes background impurity scattering in samples before irradiation. Fortunately, judging by very low pinning, this correction is negligible [26]. Also, note that this dimensionless rate contains unmodified  $T_{c0}$ , which is different from the original Abrikosov-Gor'kov definition [85].

Figure 7 shows the normalized change in superconducting transition temperature,  $\Delta t_c \equiv (T_c - T_{c0})/T_{c0}$ , as a function of the dimensionless scattering rate  $g$ . Figure 7(a) compares  $\text{V}_3\text{Si}$  single crystal with known nodeless and nodal  $s_{\pm}$  superconductors, isovalently substituted  $\text{Ba}(\text{Fe}_{0.76}\text{Ru}_{0.24})_2\text{As}_2$  and  $\text{BaFe}_2(\text{As}_{0.7}\text{P}_{0.3})_2$ , and hole-doped underdoped  $\text{Ba}_{0.81}\text{K}_{0.19}\text{Fe}_2\text{As}_2$  and optimally doped  $\text{Ba}_{0.66}\text{K}_{0.34}\text{Fe}_2\text{As}_2$  (BaK122) [42]. The theoretical curves from Eq. (8) are shown by different line types. Clearly, all sign-changing  $s_{\pm}$  superconductors show a suppression rate significantly higher than that in two-gap  $\text{V}_3\text{Si}$ , which is con-

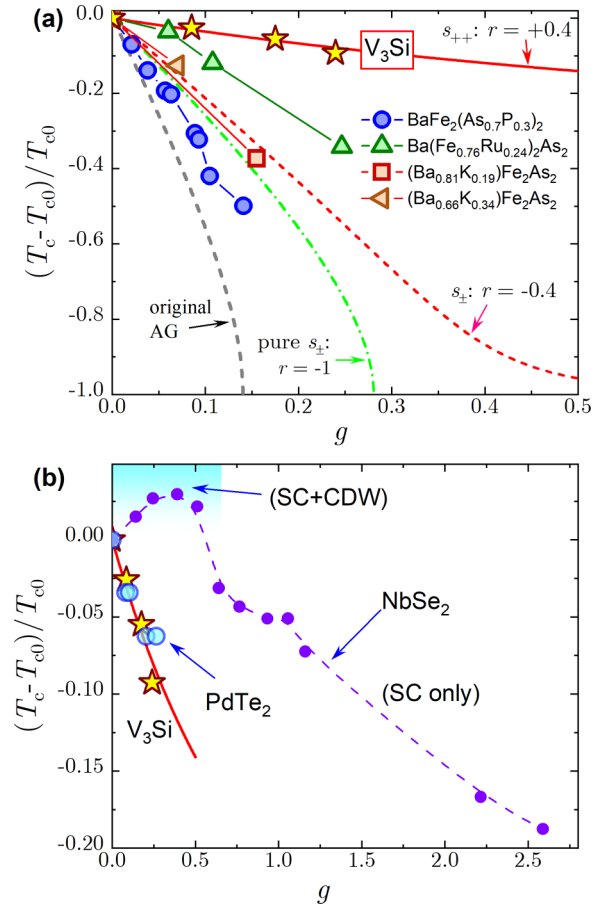


FIG. 7. Normalized change in superconducting transition temperature,  $\Delta t_c \equiv (T_c - T_{c0})/T_{c0}$ , as a function of the dimensionless scattering rate  $g$ . (a) Comparison of  $\text{V}_3\text{Si}$  single crystal with known nodeless and nodal  $s_{\pm}$  superconductors shown in the legend. The theoretical curves from Eq. (8) are shown by line types. Clearly, all sign-changing  $s_{\pm}$  superconductors show a suppression rate larger than that in  $\text{V}_3\text{Si}$ . (b) Similar comparison with another  $s_{++}$  two-band superconductor,  $\text{NbSe}_2$  [91], and an unconventional Dirac semimetal compound,  $\text{PdTe}_2$  [43,92]. As soon as the CDW is suppressed,  $\text{NbSe}_2$  shows a similar suppression rate to that of  $\text{V}_3\text{Si}$ . AG, Abrikosov-Gor'kov.

sistent with the  $s_{++}$  theoretical curve for gap ratio  $r = +0.4$ , while the same gap ratio, but of opposite sign,  $r = -0.4$ , is close to the BaK122 data. Interestingly, a nodal multi-band  $s_{\pm}$  superconductor,  $\text{BaFe}_2(\text{As}_{0.7}\text{P}_{0.3})_2$ , shows an even greater rate of  $T_c$  suppression, most likely because in this case the interband and in-band scattering channels are both pair breaking. Figure 7(b) compares  $\text{V}_3\text{Si}$  with another  $s_{++}$  two-band superconductor,  $\text{NbSe}_2$  [91], and an unconventional Dirac semimetal compound,  $\text{PdTe}_2$  [43,92]. In  $\text{NbSe}_2$ , the situation is complicated by the charge density wave (CDW), whose competition with superconductivity (SC) leads to the initial increase in  $T_c$ . However, as soon as the CDW is destroyed by disorder, further suppression of  $T_c$  is quite similar to that in our subject compound,  $\text{V}_3\text{Si}$  [91]. The second compound, unconventional  $\text{PdTe}_2$ , shows a rate of suppression quite similar to that of  $\text{V}_3\text{Si}$ . Moreover, it also has a fully gapped Fermi surface leading to exponential attenuation of the penetration depth. However, peculiarities of the



electronic band structure of PdTe<sub>2</sub> support an unconventional pairing mechanism [43,92], whereas V<sub>3</sub>Si does not have such topological features and is consistent with BCS-type two-gap superconductivity. This is a good example showing that, sometimes, thermodynamic measurements alone cannot fully answer the type-of-pairing question. They must be supported by the theoretical analysis based on the material's electronic band structure.

#### IV. CONCLUSIONS

We used controlled pointlike disorder induced by 2.5-MeV electron irradiation at different doses to study the superconducting order parameter in a V<sub>3</sub>Si single crystal. Simultaneous measurements of London penetration depth and superconducting transition temperature  $T_c$  set stringent experimental boundaries on possible superconducting states. Specifically, we observe (1) exponentially attenuated low-temperature behavior of  $\lambda(T)$  (which means a fully gapped Fermi surface), (2) a kink at higher reduced temperatures (signaling two barely coupled gaps), and (3) a significant shift in  $T_c$  (signaling gaps of different amplitude). The discussed analysis is

applicable for any choice of  $\lambda(0)$ . Using a two-band analysis for the quantities of both  $\rho_s(T)$  and  $\Delta T_c$ , we conclude that  $s_{++}$  pairing with two barely coupled gaps of different amplitudes,  $\Delta_1(0) \approx 2.53$  meV and  $\Delta_2(0) \approx 1.42$  meV, provides an excellent fit and overall self-consistent description of the experiment. This makes V<sub>3</sub>Si the earliest (superconductivity discovered in 1953) proven  $s_{++}$  superconductor, preceding MgB<sub>2</sub> (superconductivity discovered in 2001) by half a century.

#### ACKNOWLEDGMENTS

We thank David Christen for providing excellent single crystals well characterized in his earlier papers. This work was supported by the U.S. Department of Energy (DOE), Office of Science, Basic Energy Sciences, Materials Science and Engineering Division. Ames Laboratory is operated for the U.S. DOE by Iowa State University under Contract No. DE-AC02-07CH11358. The authors acknowledge support from the EMIR&A French network (FR CNRS 3618) on the ‘‘SIRIUS’’ platform under Proposal No. 18-5155. We thank the whole SIRIUS team, O. Cavani, B. Boizot, V. Metayer, and J. Losco, for operating the electron irradiation facility.

- 
- [1] G. F. Hardy and J. K. Hulm, *Phys. Rev.* **89**, 884 (1953).
  - [2] J. W. Blezjus and J. P. Carbotte, *Phys. Rev. B* **33**, 3509 (1986).
  - [3] W. D. Wu, A. Keren, L. P. Le, G. M. Luke, B. J. Sternlieb, Y. J. Uemura, D. C. Johnston, B. K. Cho, and P. Gehring, *Hyperfine Interact.* **86**, 615 (1994).
  - [4] L. R. Testardi, J. M. Poate, and H. J. Levinstein, *Phys. Rev. B* **15**, 2570 (1977).
  - [5] R. Viswanathan and R. Caton, *Phys. Rev. B* **18**, 15 (1978).
  - [6] M. N. Khlopin, *JETP Lett.* **69**, 26 (1999).
  - [7] V. G. Kogan, C. Martin, and R. Prozorov, *Phys. Rev. B* **80**, 014507 (2009).
  - [8] S. Tanaka, A. Miyake, B. Salce, D. Braithwaite, T. Kagayama, and K. Shimizu, *J. Phys.: Conf. Ser.* **200**, 012202 (2010).
  - [9] I. B. Goldberg and M. Weger, *J. Phys., Colloq.* **33**, C3-223 (1972).
  - [10] B. M. Klein, L. L. Boyer, D. A. Papaconstantopoulos, and L. F. Mattheiss, *Phys. Rev. B* **18**, 6411 (1978).
  - [11] J. Bok and J. Bouvier, *J. Supercond. Novel Magn.* **25**, 657 (2012).
  - [12] J. Nagamatsu, N. Nakagawa, T. Muranaka, Y. Zenitani, and J. Akimitsu, *Nature (London)* **410**, 63 (2001).
  - [13] F. Bouquet, Y. Wang, R. A. Fisher, D. G. Hinks, J. D. Jorgensen, A. Junod, and N. E. Phillips, *Europhys. Lett.* **56**, 856 (2001).
  - [14] J. Kortus, I. I. Mazin, K. D. Belashchenko, V. P. Antropov, and L. L. Boyer, *Phys. Rev. Lett.* **86**, 4656 (2001).
  - [15] S. L. Bud'ko, G. Lapertot, C. Petrovic, C. E. Cunningham, N. Anderson, and P. C. Canfield, *Phys. Rev. Lett.* **86**, 1877 (2001).
  - [16] J. Bardeen, L. N. Cooper, and J. R. Schrieffer, *Phys. Rev.* **106**, 162 (1957).
  - [17] V. A. Moskalenko, *Fiz. Met. Metalloved.* **8**, 503 (1959); V. A. Moskalenko, M. E. Palistrant, and V. M. Vakalyuk, *Usp. Fiz. Nauk* **161**, 155 (1991).
  - [18] H. Suhl, B. T. Matthias, and L. R. Walker, *Phys. Rev. Lett.* **3**, 552 (1959).
  - [19] B. T. Geilikman, R. O. Zaitsev, and V. Z. Kresin, *Sov. Phys. - Solid State (Engl. Transl.)* **9**, 642-7 (1967).
  - [20] I. Mazin, A. Liechtenstein, C. Rodriguez, O. Jepsen, and O. Andersen, *Phys. C (Amsterdam)* **209**, 125 (1993).
  - [21] A. Golubov, O. Dolgov, E. Maksimov, I. Mazin, and S. Shulga, *Phys. C (Amsterdam)* **235-240**, 2383 (1994).
  - [22] A. Golubov and I. Mazin, *Phys. C (Amsterdam)* **243**, 153 (1995).
  - [23] A. A. Golubov and I. I. Mazin, *Phys. Rev. B* **55**, 15146 (1997).
  - [24] R. Viswanathan, R. Caton, and C. S. Pande, *Phys. Rev. Lett.* **41**, 906 (1978).
  - [25] T. P. Orlando, E. J. McNiff, S. Foner, and M. R. Beasley, *Phys. Rev. B* **19**, 4545 (1979).
  - [26] V. G. Kogan, P. Miranović, L. Dobrosavljević-Grujić, W. E. Pickett, and D. K. Christen, *Phys. Rev. Lett.* **79**, 741 (1997).
  - [27] R. Prozorov and V. G. Kogan, *Rep. Prog. Phys.* **74**, 124505 (2011).
  - [28] M. Zehetmayer and J. Hecher, *Supercond. Sci. Technol.* **27**, 044006 (2014).
  - [29] H. Kim, K. Cho, M. A. Tanatar, V. Taufour, S. K. Kim, S. L. Bud'ko, P. C. Canfield, V. G. Kogan, and R. Prozorov, *Symmetry* **11**, 1012 (2019).
  - [30] Yu. A. Nefyodov, A. M. Shuvaev, and M. R. Trunin, *Europhys. Lett.* **72**, 638 (2005).
  - [31] A. Perucchi, D. Nicoletti, M. Ortolani, C. Marini, R. Sopracase, S. Lupi, U. Schade, M. Putti, I. Pallecchi, C. Tarantini, M. Ferretti, C. Ferdeghini, M. Monni, F. Bernardini, S. Massidda, and P. Dore, *Phys. Rev. B* **81**, 092509 (2010).
  - [32] S. Tanaka, Handoko, A. Miyake, T. Kagayama, K. Shimizu, A. Böhmer, P. Burger, F. Hardy, C. Meingast, T. Tsutsami, and Y. Onuki, *J. Phys. Soc. Jpn.* **81**, SB026 (2012).
  - [33] L. R. Testardi and T. B. Bateman, *Phys. Rev.* **154**, 402 (1967).
  - [34] A. Carrington, *C. R. Phys.* **12**, 502 (2011).

- [35] V. G. Kogan and R. Prozorov, *Phys. Rev. B* **93**, 224515 (2016).
- [36] D. J. van Harlingen, *Rev. Mod. Phys.* **67**, 515 (1995).
- [37] A. A. Golubov and I. I. Mazin, *Appl. Phys. Lett.* **102**, 032601 (2013).
- [38] S. Sykora and P. Coleman, *Phys. Rev. B* **84**, 054501 (2011).
- [39] T. Hanaguri, S. Niitaka, K. Kuroki, and H. Takagi, *Science* **328**, 474 (2010).
- [40] D. V. Efremov, M. M. Korshunov, O. V. Dolgov, A. A. Golubov, and P. J. Hirschfeld, *Phys. Rev. B* **84**, 180512(R) (2011).
- [41] G. Ghigo, D. Torsello, G. A. Ummarino, L. Gozzelino, M. A. Tanatar, R. Prozorov, and P. C. Canfield, *Phys. Rev. Lett.* **121**, 107001 (2018).
- [42] K. Cho, M. Kończykowski, S. Teknowijoyo, M. A. Tanatar, and R. Prozorov, *Supercond. Sci. Technol.* **31**, 064002 (2018).
- [43] S. Teknowijoyo, N. H. Jo, M. S. Scheurer, M. A. Tanatar, K. Cho, S. L. Bud'ko, P. P. Orth, P. C. Canfield, and R. Prozorov, *Phys. Rev. B* **98**, 024508 (2018).
- [44] E. H. Krenkel, M. A. Tanatar, M. Kończykowski, R. Grasset, E. I. Timmons, S. Ghimire, K. R. Joshi, Y. Lee, L. Ke, S. Chen, C. Petrovic, P. P. Orth, M. S. Scheurer, and R. Prozorov, [arXiv:2110.02025](https://arxiv.org/abs/2110.02025).
- [45] F. Gross, B. S. Chandrasekhar, D. Einzel, K. Andres, P. J. Hirschfeld, H. R. Ott, J. Beuers, Z. Fisk, and J. L. Smith, *Z. Phys. B: Condens. Matter* **64**, 175 (1986).
- [46] F. Gross-Alltag, B. S. Chandrasekhar, D. Einzel, P. J. Hirschfeld, and K. Andres, *Z. Phys. B: Condens. Matter* **82**, 243 (1991).
- [47] Y. Mizukami, M. Kończykowski, Y. Kawamoto, S. Kurata, S. Kasahara, K. Hashimoto, V. Mishra, A. Kreisel, Y. Wang, P. J. Hirschfeld, Y. Matsuda, and T. Shibauchi, *Nat. Commun.* **5**, 5657 (2014).
- [48] S. Ghimire, M. Kończykowski, K. Cho, M. A. Tanatar, D. Torsello, I. S. Veshchunov, T. Tamegai, G. Ghigo, and R. Prozorov, *Materials* **14**, 3267 (2021).
- [49] T. Takenaka, Y. Mizukami, J. A. Wilcox, M. Kończykowski, S. Seiro, C. Geibel, Y. Tokiwa, Y. Kasahara, C. Putzke, Y. Matsuda, A. Carrington, and T. Shibauchi, *Phys. Rev. Lett.* **119**, 077001 (2017).
- [50] K. Cho, M. Kończykowski, S. Teknowijoyo, M. A. Tanatar, Y. Liu, T. A. Lograsso, W. E. Straszheim, V. Mishra, S. Maiti, P. J. Hirschfeld, and R. Prozorov, *Sci. Adv.* **2**, e1600807 (2016).
- [51] M. Putti, M. Affronte, C. Ferdeghini, P. Manfrinetti, C. Tarantini, and E. Lehmann, *Phys. Rev. Lett.* **96**, 077003 (2006).
- [52] M. B. Schilling, A. Baumgartner, B. Gorshunov, E. S. Zhukova, V. A. Dravin, K. V. Mitsen, D. V. Efremov, O. V. Dolgov, K. Iida, M. Dressel, and S. Zapf, *Phys. Rev. B* **93**, 174515 (2016).
- [53] J. Kim, N. Haberkorn, M. J. Graf, I. Usov, F. Ronning, L. Civale, E. Nazaretski, G. F. Chen, W. Yu, J. D. Thompson, and R. Movshovich, *Phys. Rev. B* **86**, 144509 (2012).
- [54] M. Yethiraj, D. K. Christen, D. McK. Paul, P. Miranovic, and J. R. Thompson, *Phys. Rev. Lett.* **82**, 5112 (1999).
- [55] M. Yethiraj, D. K. Christen, A. A. Gapud, D. M. Paul, S. J. Crowe, C. D. Dewhurst, R. Cubitt, L. Porcar, and A. Gurevich, *Phys. Rev. B* **72**, 060504(R) (2005).
- [56] R. Prozorov and R. W. Giannetta, *Supercond. Sci. Technol.* **19**, R41 (2006).
- [57] C. T. Van Degrift, *Rev. Sci. Instrum.* **46**, 599 (1975).
- [58] R. Prozorov, R. W. Giannetta, A. Carrington, and F. M. Araujo-Moreira, *Phys. Rev. B* **62**, 115 (2000).
- [59] R. Prozorov, R. W. Giannetta, A. Carrington, P. Fournier, R. L. Greene, P. Guptasarma, D. G. Hinks, and A. R. Banks, *Appl. Phys. Lett.* **77**, 4202 (2000).
- [60] R. Prozorov, *Phys. Rev. Appl.* **16**, 024014 (2021).
- [61] R. Prozorov, M. Kończykowski, M. A. Tanatar, A. Thaler, S. L. Bud'ko, P. C. Canfield, V. Mishra, and P. J. Hirschfeld, *Phys. Rev. X* **4**, 041032 (2014).
- [62] A. C. Damask and G. J. Dienes, *Point Defects in Metals* (Gordon and Breach, New York, 1963).
- [63] M. W. Thompson, *Defects and Radiation Damage in Metals*, Cambridge Monographs on Physics (Cambridge University Press, Cambridge, 1974).
- [64] J. P. Perdew, K. Burke, and M. Ernzerhof, *Phys. Rev. Lett.* **77**, 3865 (1996).
- [65] S. Tanaka, A. Miyake, T. Kagayama, and K. Shimizu, *J. Phys.: Conf. Ser.* **273**, 012105 (2011).
- [66] G. Kresse and J. Furthmüller, *Phys. Rev. B* **54**, 11169 (1996).
- [67] K. D. Belashchenko, M. van Schilfgaarde, and V. P. Antropov, *Phys. Rev. B* **64**, 092503 (2001).
- [68] D. Torsello, G. A. Ummarino, J. Bekaert, L. Gozzelino, R. Gerbaldo, M. A. Tanatar, P. C. Canfield, R. Prozorov, and G. Ghigo, *Phys. Rev. Appl.* **13**, 064046 (2020).
- [69] B. Sadigh and V. Ozoliņš, *Phys. Rev. B* **57**, 2793 (1998).
- [70] A. Matthiessen and C. Vogt, *Philos. Trans. R. Soc. London* **154**, 167 (1864).
- [71] T. Hanaguri, Y. Iino, A. Maeda, and T. Fukase, *Phys. C (Amsterdam)* **246**, 223 (1995).
- [72] T. J. Greytak and J. H. Wernick, *J. Phys. Chem. Solids* **25**, 535 (1964).
- [73] Y. Muto, N. Toyota, K. Noto, K. Akutsu, M. Isino, and T. Fukase, *J. Low Temp. Phys.* **34**, 617 (1979).
- [74] M. Li, N. R. Lee-Hone, S. Chi, R. Liang, W. N. Hardy, D. A. Bonn, E. Girt, and D. M. Broun, *New J. Phys.* **18**, 082001 (2016).
- [75] J. D. Fletcher, A. Carrington, O. J. Taylor, S. M. Kazakov, and J. Karpinski, *Phys. Rev. Lett.* **95**, 097005 (2005).
- [76] R. D. Brown and J. R. Cost, *JOM* **42**, 39 (1990).
- [77] H. W. Weber, in *Advances in Cryogenic Engineering Materials* (Springer, New York, 1986), pp. 853–864.
- [78] T. Tamegai, T. Taen, H. Yagyuda, Y. Tsuchiya, S. Mohan, T. Taniguchi, Y. Nakajima, S. Okayasu, M. Sasase, H. Kitamura, T. Murakami, T. Kambara, and Y. Kanai, *Supercond. Sci. Technol.* **25**, 084008 (2012).
- [79] The SIRIUS linear accelerator, <https://portail.polytechnique.edu/lsi/en/facilities/sirius-installation>.
- [80] O. S. Oen, Cross sections for atomic displacements in solids by fast electrons, technical report, Office of Scientific and Technical Information (OSTI), ID No. 4457758, Report No. ORNL-4897 (1973).
- [81] P. Anderson, *J. Phys. Chem. Solids* **11**, 26 (1959).
- [82] M. Tinkham, *Introduction to Superconductivity*, 2nd ed., Dover Books on Physics (Dover, Mineola, NY, 2004).
- [83] V. G. Kogan, *Phys. Rev. B* **66**, 020509(R) (2002).
- [84] V. G. Kogan, R. Prozorov, and A. E. Koshelev, *Phys. Rev. B* **100**, 014518 (2019).
- [85] A. A. Abrikosov and L. P. Gor'kov, *Zh. Eksp. Teor. Fiz.* **39**, 1781 (1960) [*Sov. Phys. JETP* **12**, 1243 (1961)].

- [86] L. A. Openov, *JETP Lett.* **66**, 661 (1997).
- [87] L. A. Openov, *Phys. Rev. B* **69**, 224516 (2004).
- [88] S. A. Alterovitz, D. E. Farrell, B. S. Chandrasekhar, E. J. Haugland, J. W. Blue, and D. C. Liu, *Phys. Rev. B* **24**, 90 (1981).
- [89] A. A. Abrikosov, L. P. Gor'kov, and I. E. Dzyaloshinskii, *Methods of Quantum Field Theory in Statistical Physics* (Englewood Cliffs, N.J., Prentice-Hall, 1963).
- [90] V. G. Kogan, *Phys. Rev. B* **87**, 220507(R) (2013).
- [91] K. Cho, M. Kończykowski, S. Teknowijoyo, M. A. Tanatar, J. Guss, P. B. Gartin, J. M. Wilde, A. Kreyssig, R. J. McQueeney, A. I. Goldman, V. Mishra, P. J. Hirschfeld, and R. Prozorov, *Nat. Commun.* **9**, 2796 (2018).
- [92] E. I. Timmons, S. Teknowijoyo, M. Kończykowski, O. Cavani, M. A. Tanatar, S. Ghimire, K. Cho, Y. Lee, L. Ke, N. H. Jo, S. L. Bud'ko, P. C. Canfield, P. P. Orth, M. S. Scheurer, and R. Prozorov, *Phys. Rev. Res.* **2**, 023140 (2020).